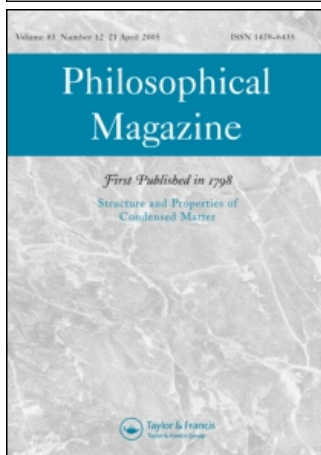


This article was downloaded by:[Forest, Samuel]
On: 31 July 2007
Access Details: [subscription number 779839453]
Publisher: Taylor & Francis
Informa Ltd Registered in England and Wales Registered Number: 1072954
Registered office: Mortimer House, 37-41 Mortimer Street, London W1T 3JH, UK



Philosophical Magazine

First published in 1798

Publication details, including instructions for authors and subscription information:
<http://www.informaworld.com/smpp/title~content=t713695589>

Ensemble averaging stress-strain fields in polycrystalline aggregates with a constrained surface microstructure - Part 1: anisotropic elastic behaviour

Online Publication Date: 01 March 2007

To cite this Article: Zeghadi, A., N'guyen, F., Forest, S., Gourgues, A. -F. and Bouaziz, O. (2007) 'Ensemble averaging stress-strain fields in polycrystalline aggregates with a constrained surface microstructure - Part 1: anisotropic elastic behaviour', *Philosophical Magazine*, 87:8, 1401 - 1424

To link to this article: DOI: 10.1080/14786430601009509

URL: <http://dx.doi.org/10.1080/14786430601009509>

PLEASE SCROLL DOWN FOR ARTICLE

Full terms and conditions of use: <http://www.informaworld.com/terms-and-conditions-of-access.pdf>

This article maybe used for research, teaching and private study purposes. Any substantial or systematic reproduction, re-distribution, re-selling, loan or sub-licensing, systematic supply or distribution in any form to anyone is expressly forbidden.

The publisher does not give any warranty express or implied or make any representation that the contents will be complete or accurate or up to date. The accuracy of any instructions, formulae and drug doses should be independently verified with primary sources. The publisher shall not be liable for any loss, actions, claims, proceedings, demand or costs or damages whatsoever or howsoever caused arising directly or indirectly in connection with or arising out of the use of this material.

© Taylor and Francis 2007

Ensemble averaging stress–strain fields in polycrystalline aggregates with a constrained surface microstructure – Part 1: anisotropic elastic behaviour

A. ZEGHADI†, F. N’GUYEN†, S. FOREST*†, A.-F. GOURGUES† and O. BOUAZIZ‡

†Centre des Matériaux/Mines Paris, Paristech, CNRS UMR 7633, B.P. 87, 91003 Evry Cedex, France

‡ARCELOR Research, Voie Romaine, B.P. 30320, 57283 Maizières-lès-Metz, France

(Received 7 April 2006; in final form 23 July 2006)

The effect of three-dimensional (3D) grain morphology on the deformation at a free surface in polycrystalline aggregates is investigated by means of a large-scale finite element and statistical approach. For a given two-dimensional surface at $z=0$ containing 39 grains with given crystal orientations, 17 random 3D polycrystalline aggregates are constructed having different 3D grain shapes and orientations except at $z=0$, based on an original 3D image analysis procedure. They are subjected to overall tensile loading conditions. The resulting stress–strain fields at the free surface $z=0$ are analyzed. Ensemble average and variance maps of the stress field at the observed surface are computed. In the case of an anisotropic elastic behaviour of the grains, fluctuations ranging between 5% and 60% are found in the equivalent stress level at a given material point of the observed surface from one realization of the microstructure to another. These results have important implications in the way of comparing finite element simulations and surface strain field measurements in metal polycrystals.

1. Introduction

The development of field measurement methods in the past 15 years provides us with a precise knowledge of the heterogeneity of strains, stresses (via the determination of elastic strains) and lattice rotations in metallic polycrystals [1–3]. The deformation of grids deposited on the surface specimen, interpreted by means of image correlation analysis, X-ray microdiffraction, and Electron Back-Scatter Diffraction (EBSD) are respectively used to evaluate the fields of total strain, elastic strain and lattice orientation at various stages of the deformation of polycrystals, with a pixel resolution below the micron scale [4–8]. The observation of detailed strain fields inside the individual

*Corresponding author. Email: samuel.forest@ensmp.fr

grains for a large number of grains reveals the extreme heterogeneity of deformation due to crystal slip processes. The development of bands of intense plastic deformation crossing several grains is often reported, in addition to the strong intragranular heterogeneities induced by strain incompatibilities at grain boundaries. These now standard experimental techniques can be applied at the free surface of a polycrystal subjected to various loading conditions such as tension and shear. The analysis of grid deformation usually provides the in-plane components of the displacement field, from which in-plane components of the strain tensor can be evaluated. EBSD analysis gives the full three-dimensional (3D) orientation map of all surface grains. Microdiffraction analyses using for instance synchrotron radiation provide two-dimensional (2D) maps of the 3D elastic strain tensor field for material points at the surface of polycrystals [6].

Such field measurements can be used to validate the theoretical framework of continuum crystal plasticity settled in [9, 10]. The results of finite element simulations based on the numerical integration of the constitutive equations for single crystals can be compared to the corresponding experimental information [5, 6, 11–13]. Continuum crystal plasticity takes the crystallographic nature of plastic slip into account via a set of slip variables γ^s associated with each slip system s . The first finite element simulations of the elastic-viscoplastic behaviour of polycrystals go back to [11, 14–17] in which two-dimensional analyses of the problem are proposed. With a view to more realistic simulations and more accurate comparisons with the experimental results, a trend towards 3D finite element modelling of polycrystals has been observed since the early 1990s [5, 12, 18–23]. The usual strategy for a direct comparison between strain field measurements and finite element results consists in producing a finite element mesh of the surface morphology of the observed grains and subjecting it to boundary conditions as close as possible to the experimental ones. A 2D finite element mesh of the grains is generally obtained starting from the EBSD map of the considered surface which simultaneously provides the orientation map of the grains and the location of grain boundaries. In most cases, the actual 3D morphology of the considered surface grains remains unknown and specific assumptions have to be made for the finite element simulations. A 3D mesh of the polycrystalline sample can be obtained by simple extension of the 2D mesh with respect to the normal direction, in the case of quasi-columnar grains [7, 23], or by interpolating the grain shape from the intersection of the grains with the other free surfaces of the sample in the case of large recrystallized grains [6, 11]. In these simulations, grain boundaries are perfect interfaces with continuity of displacement and traction vectors. No grain boundary migration is accounted for. Grain boundaries are regarded as pure sources of strain incompatibilities between grains which induce strong strain heterogeneities.

The main problem in assessing the quality of the simulation results compared to the available experimental data such as strain and lattice rotation fields lies in the fact that the usually unknown actual 3D morphology of the grains can significantly affect the strain and lattice rotation fields at the surface. As a result, only uncertain and incomplete validation of the continuum models can be gained from direct comparison of the experimental and simulated fields. The discrepancy

between computation and observation in some grains is usually attributed to at least three reasons:

- (1) Insufficient refinement of the finite element mesh; effects of mesh sensitivity have already been analyzed in [21, 24]. Coarse meshes are sufficient to obtain a correct estimation of the overall response. In contrast, very fine meshes are required to get a detailed and converged description of the intragranular fields.
- (2) Physical relevance of the constitutive equations; the objective of the present paper is not to show the relevance of the continuum crystal plasticity model which has already been demonstrated at least in the case of large grains in multicrystals; indeed, the fact that good correlations are reported in the literature between model and field measurements when the grain morphology is exactly known [5, 11, 12], indicates that available constitutive equations can be trusted, at least in the case of large grains for which size effects can be excluded.
- (3) Uncertainty in the actual 3D morphology of the observed grains [18, 25]; it seems that no systematic study has been performed to quantify the impact of the 3D grain morphology on the fluctuations of stress and strain at a given surface of a polycrystal. At least, in [26], the responses of a columnar microstructure and of a random polycrystal are compared for a given 2D grain repartition and lattice orientation map at one free surface. Huge differences in local plastic strain values at the free surface are reported at the same overall loading stage.

In the present work, a large-scale computational and statistical approach is developed to give a quantitative assessment of the bias introduced in the estimation of surface stress–strain and lattice rotation fields, by the incomplete knowledge of the 3D grain morphology below a given surface with fixed 2D grain morphology. It aims at estimating the fluctuations of plastic strain on a free surface with fixed 2D grain morphology and orientations when the 3D shape of the grains below the surface are changed. This is a question often raised in the interpretation of strain field measurements at the surface of deformed polycrystals. There is currently no precise answer in the literature to this question. For explicit comparison with experimental results, the assumption of columnar morphology is usually made in the computations. We show in the present work that this introduces a strong bias in the estimation of strain fields. To give a quantitative answer to the previous question, the following tools are needed:

- (1) an image analysis algorithm to produce 3D polycrystalline aggregates with a constrained 2D morphology; such an algorithm has no equivalent in the literature to the knowledge of the authors;
- (2) a statistical approach; the fluctuations can be estimated only by a sufficiently high number of simulations with different 3D grain morphologies below the constrained surface; such a strategy was not developed in the previous contributions.

The first part of this work is devoted to the presentation of the 3D polycrystalline microstructures obtained from a given set of surface grains and to the analysis of the

stress–strain heterogeneity in the case of anisotropic linear elasticity. The case of elastoplastic crystal behaviour is analyzed in part 2 of this work [27]. Random three-dimensional polycrystalline aggregates having different grain morphology and crystal orientations except at a given free surface are constructed and analyzed in section 2. The computational tools required to perform large-scale 3D finite element analyses of the deformation of polycrystalline aggregates are presented in section 3. Precise notations regarding the statistical treatment of simulation results including volume and ensemble average and variance operators are introduced in subsection 3.2. The question of the choice of the sample thickness, i.e. the number of grains within the thickness of the polycrystalline aggregates to be subjected to mechanical loading, is addressed in section 4. In section 5 the stress fields in 18 linear elastic copper polycrystalline aggregates sharing a common free surface and deformed in tension are analyzed following the systematic statistical approach defined in section 3.

2. Representation of the microstructure

The basic model retained in this work for the morphology of polycrystals is that of Voronoi polyhedra [21]. This is a simple and widely used model to represent equiaxial grains without special morphological texture [21, 24]. The Voronoi cells correspond to the uniform growth of grains nucleated at seeds dispersed in the 3D space according to a Poisson process. A repulsion distance is used to avoid too small grains. The objective of this section is to show how such a 3D Voronoi tessellation can be connected to a constrained surface microstructure.

2.1. *Original algorithm for obtaining a 3D grain distribution with a constrained surface geometry*

In this work, the reference (free) surface of polycrystalline aggregates is composed of 39 grains labelled in figure 1. This image was generated by a section of a given set of 3D Voronoi polyhedra, but could also have been obtained from EBSD analysis [28, 29]. The colour of each surface grain corresponds to a given specific crystal orientation. The objective of the algorithm presented in this section is to produce random 3D polycrystalline microstructures that share this common reference surface at $z=0$. For each realization the constructed volume is therefore located at $0 \leq z \leq H$ where H is the thickness of the polycrystalline volume. The size of images that will be produced is $200 \times 200 \times 200$ voxels (so $H=200$). The number of grains contained in the images is on average $6 \times 6 \times 6 = 216$ grains. The mean grain volume is $V_0 = 37\,037$ voxels. The mean grain size is conventionally taken as $d_0 = V_0^{1/3} \simeq 33$ voxels. The construction of the aggregates is decomposed into two main stages:

- (1) *Generation of the first layer of 3D grains starting from the reference free surface.* The first layer of voxels is made of the image of the constrained surface $z=0$ (see figure 1). It is the same for all realizations of the microstructure. The second layer of voxels is obtained from the first one by expanding or eroding each grain based on a random process. The procedure is carried out one grain after another. The erosion of one grain and the subsequent growth of the neighbouring grains are illustrated in figure 2.

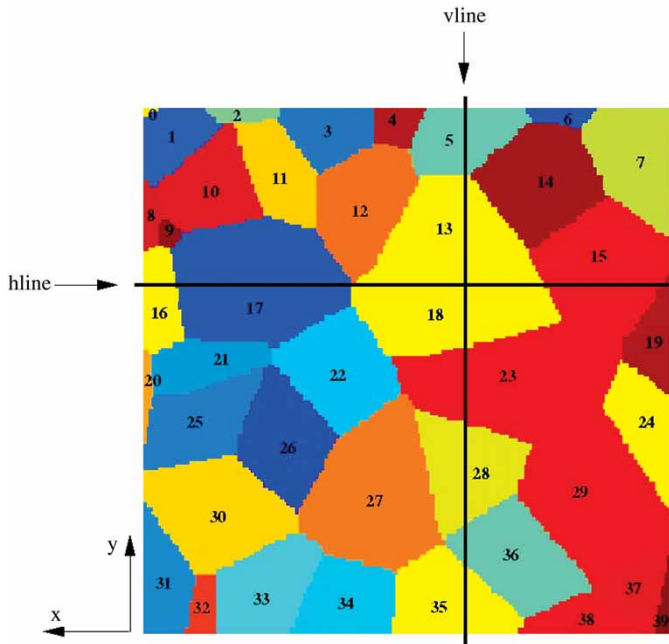


Figure 1. Reference surface $z=0$ prescribed for the construction of polycrystalline aggregates. All surface grains are labelled from 1 to 39. Two lines *hline* and *vline* have been distinguished along which mechanical variables obtained in the finite element simulations of this work have been plotted.

The initial eroded grain A is shown in figure 2a whereas the final state of this grain and its environment is shown in figure 2b. Five steps were needed to reach this final shape. They are illustrated in figure 2c. Each step corresponds to the motion of one boundary of the labelled neighbouring grains. A new grain, labelled 7 in the picture, had to be created to close this process. When a growth or reduction rate distribution has been chosen and enforced for all grains of the section, a 2D convexifying procedure is performed by replacing the obtained 2D grains by their convex envelopes. This algorithm is run again for the next layer of voxels. In the case of expanding grains, the growth rate chosen initially is kept constant for the subsequent layers until the depth $z = d_0/2$ is reached on average. Afterwards, the sign of the growth rate is changed in order to finally close the grain. This part of the algorithm stops when all the 39 initial grains have been expanded or reduced and closed. An example of the resulting microstructure is provided in figure 3a which shows a section perpendicular to the constrained surface. The section of eight grains grown from the surface $z=0$ can be seen.

- (2) *Union of the first layer of grains with of the Voronoi tessellation.* The next step consists in generating random seeds in the remaining volume of the image and in producing a Voronoi tessellation. This is done in 3D but a 2D illustration is shown in figure 3b. The voxels of the first layer of grains constructed previously is superimposed on the Voronoi tessellation made

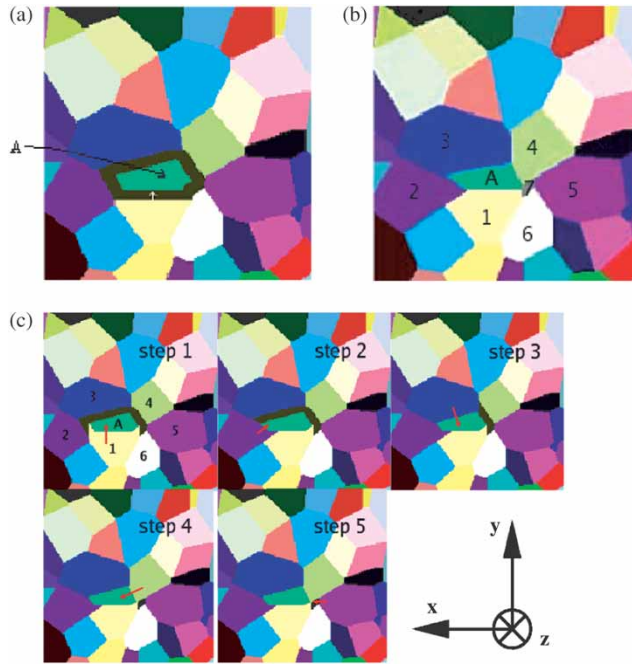


Figure 2. Erosion of a grain belonging to a given surface and its modification due to the growth of neighbouring grains: (a) the considered grain A is eroded; (b) final environment of grain A; (c) the five growth steps of the grains surrounding grain A necessary to get picture (b). The i th step of figure (c) corresponds to the normal growth of one grain boundary of neighbour grain i , as indicated by the red arrow.

of 216 grains by substituting the corresponding voxels. This procedure generally leads to unacceptable grain shapes just below the first layer of grains. That is why a final 3D convexifying process is carried out for all the grains except those of the first layer since they are already convex. The grains are replaced by their convex envelop; this convexifying procedure is run until all the grains in the volume are convex; this may require several iterations; if the procedure does not converge, the volume is excluded. The constraint of grain convexity is introduced to avoid unrealistic grain shapes and because grains are convex in the reference Voronoi model. Figure 3c shows the result of the union and convexifying process in one section perpendicular to the constrained surface.

The proposed algorithm remains heuristic and the existence of a solution for each realization of the random parameters is not ensured. In particular, the produced aggregates do not correspond strictly to a Voronoi tessellation. The surface constraint and the construction method introduce a bias in the cell distributions. Algorithms keeping the Voronoi character of the model do exist, as demonstrated in [30], but turn out to be too time-consuming in the 3D case.

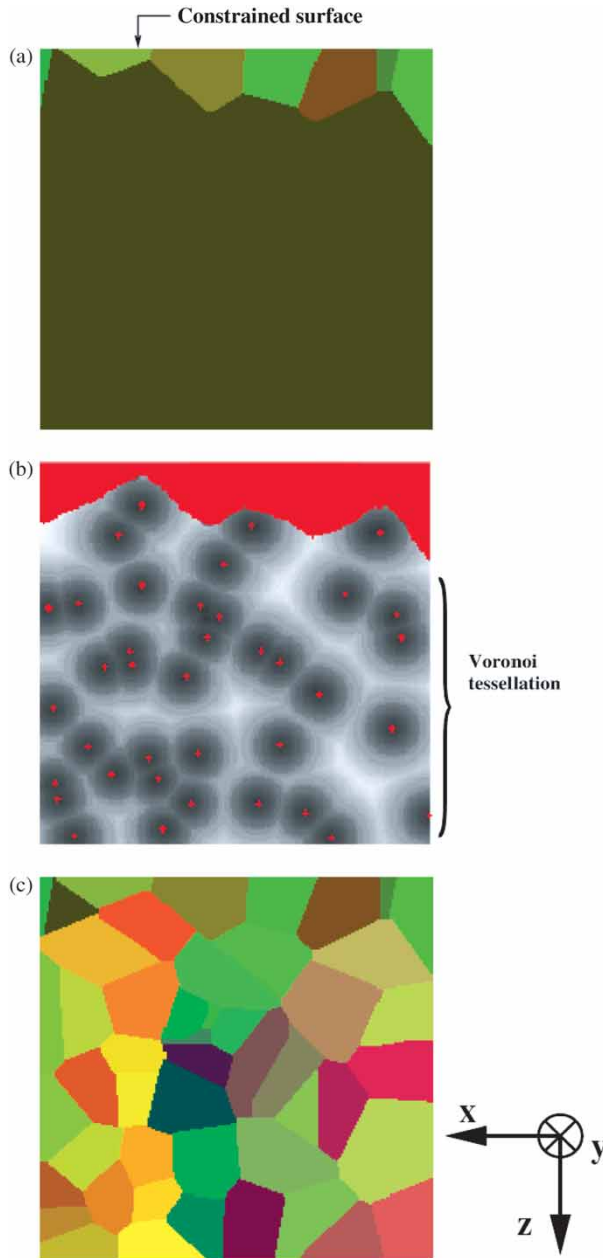


Figure 3. (a) Section, normal to direction y , of the first layer of grains below the constrained surface; (b) Voronoi tessellation of the section below the first layer of grains; the red spots denote the random seeds of the cells; the initial first layer of grains is superimposed on the image; (c) union of the first layer of grains and of the Voronoi cells. The grains have been made convex after the union of images (a) and (b). In the three images, the top horizontal line of pixels belongs to the constrained surface $z=0$.

2.2. Description of the obtained 3D polycrystalline aggregates

Seventeen polycrystalline microstructures with the constrained surface of figure 1 have been produced. Six of them are shown in figure 4. The 3D images of two of them have been cut perpendicularly to the free surface along line *hline* in figure 4a. The morphology of the grains directly below the free surface can be clearly seen. Slices perpendicular to the free surface and going through the line *hline* of figure 1 are shown for four realizations in figure 4b. The proposed algorithm leads to strongly different grain shapes below the constrained surface from one realization to another. In particular the angle between grain boundaries and the surface $z=0$ can be significantly changed from one realization to another. As a result, orange grain 18 is significantly larger in the first realization of figure 4a than in the second one. This can be seen also on the first and fourth slices of figure 4b. Red grain 15 is very small in the first slice of 4b and much larger in the fourth slice. The reverse holds for brown grain 19. These strong differences are expected to play an important role on the development of stresses at the free surface.

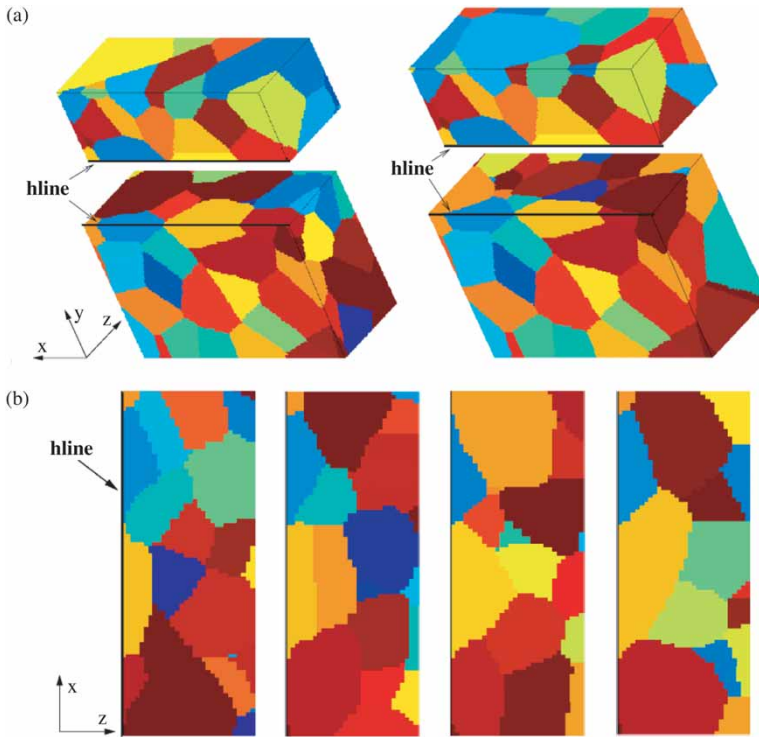


Figure 4. (a) Two realizations of polycrystalline aggregates with constrained free surface $z = 0$. The reference surface $z = 0$ is given in figure 1. The volumes have been cut into two parts along a plane perpendicular to the free surface and containing the line *hline* (in bold) of figure 1, in order to show the grain morphology below the constrained free surface. (b) Four further realizations are shown. The section plane is perpendicular to the free surface and contains *hline* (in bold).

The characteristics of the produced microstructures can be analyzed quantitatively. A histogram of grain sizes in a polycrystalline volume with constrained surface was compared to the corresponding histogram for the a realization of pure Voronoi polyhedra. The differences remain small ($<3\%$) so that the constrained microstructures do not differ essentially from Voronoi polyhedra. This statement is confirmed by the analysis of average grain size and variance in sections parallel to the constrained free surface $z=0$ as a function of the coordinate z . The grain size close to the free surface does not differ significantly from the size of grains far from the surface, as shown in [31].

Finally, the constructed microstructures are available for subsequent mechanical computations carried out in the case of elasticity in this part and in the nonlinear case in part 2 of this work [27]. Another grain morphology will be useful to assess the results based on the previous random microstructures, namely, the columnar microstructure deduced from the surface image of figure 1 by translation along z , and shown in figure 5.

3. Computational methods

3.1. Finite element meshing and parallel computing

All the aggregates are constrained to share the common surface at $z=0$. Fixed crystal orientations are attributed to the 39 grains of the constrained surface according to table 1. They are unchanged from one realization to another. The orientations of the remaining grains in the 3D aggregates are chosen randomly and differ from one realization to another. The target crystallographic texture is isotropic.

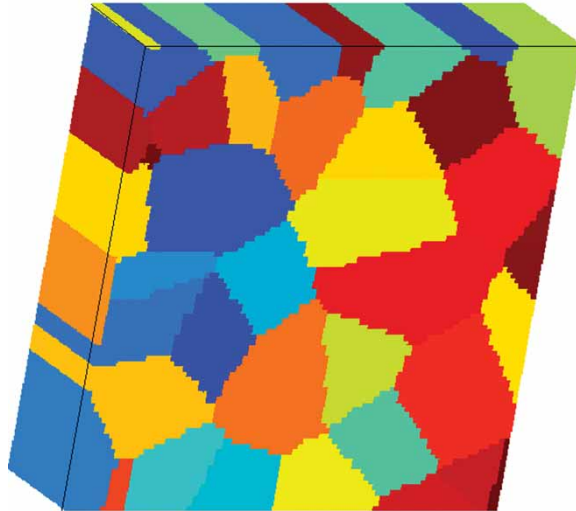


Figure 5. Columnar grains deduced from the reference surface of figure 1. All grain boundaries are perpendicular to the constrained surface.

Table 1. Crystal orientations of the 39 grains of the reference surface of figure 1. Euler–Bunge angles (in degrees) are given with respect to the reference frame of the sample (x, y, z) defined in figure 1.

Grain number	ϕ_1	Φ	ϕ_2
1	278.4	85.9	180.2
2	35.0	112.4	49.0
3	210.1	57.0	311.9
4	352.8	120.1	231.6
5	358.2	118.3	285.3
6	244.3	60.1	315.9
7	53.3	138.3	244.5
8	73.7	31.7	70.7
9	344.0	58.7	28.8
10	296.0	117.9	98.8
11	160.7	81.7	268.5
12	118.3	52.3	60.9
13	260.9	18.1	45.7
14	179.6	135.6	271.9
15	120.1	48.2	73.9
16	174.4	65.5	95.4
17	185.2	74.5	44.5
18	225.6	39.9	162.7
19	58.5	85.6	246.2
20	117.1	94.5	230.7
21	95.1	130.9	97.3
22	152.8	66.2	49.9
23	124.4	63.4	250.5
24	251.9	31.7	141.8
25	110.1	46.7	254.0
26	261.8	121.8	286.0
27	317.2	116.3	355.1
28	193.2	67.4	43.1
29	223.4	77.1	53.9
30	210.8	52.4	240.5
31	214.7	77.7	108.2
32	152.5	72.2	272.4
33	116.1	85.4	130.6
34	12.6	118.5	76.8
35	279.7	135.2	314.3
36	160.1	35.1	261.4
37	0.1	90.0	253.9
38	8.0	110.2	301.7
39	342.7	133.0	252.8

The multiphase element technique is used to obtain a finite element mesh from the images of microstructures produced in the previous sections. This technique was initially proposed in [32] and extensively used for the computation of elastoplastic polycrystalline aggregates [21]. It consists in superimposing a regular finite element grid on the image of the microstructure. The constitutive behaviour at each integration point corresponds to the colour of the voxel it belongs to. In the images of the polycrystalline microstructures each colour indicates the crystal orientation

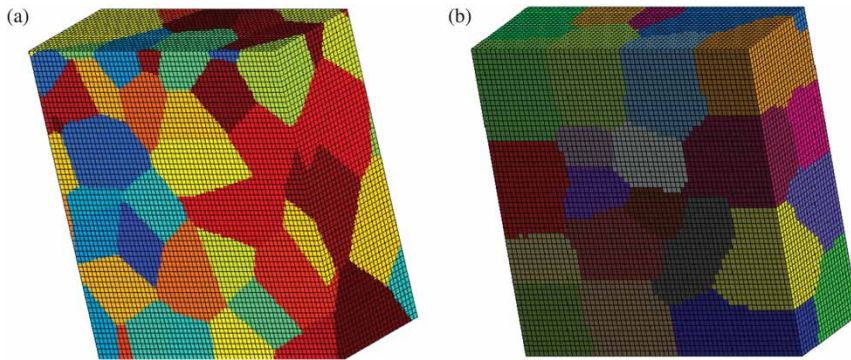


Figure 6. (a) Multiphase finite element mesh superimposed on the image of a polycrystalline aggregate with constrained free surface; (b) decomposition of the mesh into 30 subdomains for parallel computing.

of a grain. The constitutive equations are the same for all integration points of the mesh but the initial lattice orientation differs from grain to grain.

The finite elements used in this work are quadratic bricks with 20 nodes and 27 integration points. As a consequence of the multiphase element technique, integration points belonging to the same element may possess different crystal orientations. This is known to provide a poor description of grain boundaries. However, the quality of the description of the variables close to grain boundaries can be restored if the number of elements per grain is sufficiently high [22, 24]. An example of a regular mesh made of $60 \times 60 \times 21$ quadratic elements superimposed on the image of a polycrystalline aggregate is shown in figure 6a.

The numerical cost of the computations with such huge meshes is very high. The number of degrees of freedom (d.o.f.) of the typical mesh of figure 6a is close to 1 000 000. The resolution of such problems in reasonable time requires parallel computing. The parallel version of the finite element code Zset is presented in [33, 34]. The problem is solved with the FETI (Finite Element Tearing and Interconnecting) method. The parallelization scheme is based on a domain decomposition algorithm. The finite element mesh is thus decomposed into several domains (see for instance the decomposition into thirty subdomains in figure 6b). Data exchange between the different tasks uses a PVM communication protocol. A cluster of 34 Linux 1.2 GHz PCs was used in this work for the largest computation. It corresponds to 29 Go (Gigaoctets of Gigabytes) memory needed to solve the largest problem.

3.2. Ensemble averaging and dispersion operators

In this subsection, average and variance operators are defined, that will be applied to the mechanical field variables computed in this work. A limited domain V in the physical space is considered. The volume (spatial) average $\langle f \rangle$ of the field quantity f over volume V is defined as

$$\langle f \rangle := \frac{1}{V} \int_V f \, dV \quad (1)$$

When applied to the stress field component σ_{22} or strain field component ε_{22} , the application of the average volume operator gives, for a given volume V :

$$\Sigma_{22} := \langle \sigma_{22} \rangle = \frac{1}{V} \int_V \sigma_{22} dV, \quad E_{22} := \langle \varepsilon_{22} \rangle = \frac{1}{V} \int_V \varepsilon_{22} dV \quad (2)$$

The ensemble averaging operator \bar{f} for N realizations of the field f is defined as

$$\bar{f} := \frac{1}{N} \sum_{i=1}^N f^i \quad (3)$$

where f^i is the i th realization of f . This operator will be applied to the von Mises equivalent stress, at a material point \mathbf{x} for N realizations:

$$\overline{\sigma_{\text{eq}}}(\mathbf{x}) := \frac{1}{N} \sum_{i=1}^N \sigma_{\text{eq}}^i(\mathbf{x}), \quad \text{with } \sigma_{\text{eq}} := \sqrt{\frac{3}{2} \sigma^{\text{dev}} : \sigma^{\text{dev}}} \quad (4)$$

where σ^{dev} is the deviatoric part of the stress tensor σ . Ensemble averaging can also be applied to volume averaged quantities such as the global stress component Σ_{22} :

$$\overline{\Sigma_{22}} := \frac{1}{N} \sum_{i=1}^N \Sigma_{22}^i = \frac{1}{N} \sum_{i=1}^N \langle \sigma_{22} \rangle_i = \frac{1}{N} \sum_{i=1}^N \frac{1}{V} \int_{V_i} \sigma_{22}^i dV \quad (5)$$

where σ_{22}^i is the i th realization of the field $\sigma_{22}(\mathbf{x})$. The variance of a random variable f is denoted by $D(f)$. The relative variance is obtained by dividing the variance by the ensemble average value:

$$D(f) := \sqrt{\frac{1}{N} \sum_{i=1}^N (f^i - \bar{f})^2}, \quad \epsilon(f) = \frac{D(f)}{\bar{f}} \quad (6)$$

The square of the variance of the von Mises equivalent stress and its relative variance at point \mathbf{x} are therefore

$$D^2(\sigma_{\text{eq}}(\mathbf{x})) = \frac{1}{N} \sum_{i=1}^N (\sigma_{\text{eq}}^i(\mathbf{x}) - \overline{\sigma_{\text{eq}}}(\mathbf{x}))^2, \quad \epsilon(\sigma_{\text{eq}}(\mathbf{x})) = \frac{D(\sigma_{\text{eq}}(\mathbf{x}))}{\overline{\sigma_{\text{eq}}}(\mathbf{x})} \quad (7)$$

4. Estimating the range of elastic stresses

In this section, several characteristics of the finite element computations to be performed in section 5.1 are settled, namely, boundary conditions, mesh density and sample thickness. The latter issue is of strong mechanical importance: How many grains within the thickness of the sample do affect the stress field at the constrained surface?

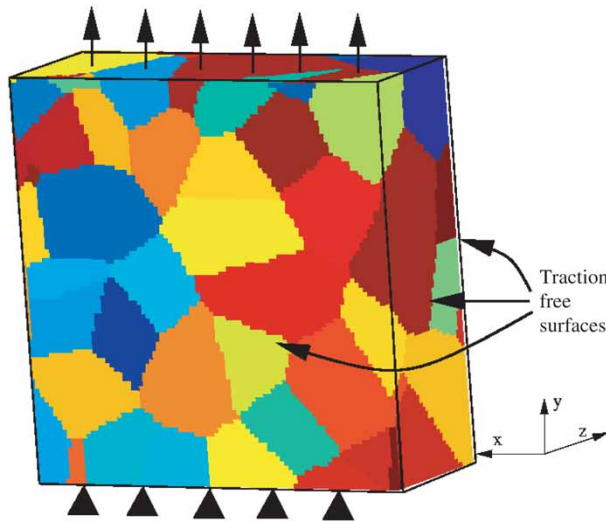


Figure 7. Boundary value problem for the tension of a polycrystalline aggregate with a given surface morphology $z=0$.

4.1. Position of the boundary value problem

All considered polycrystalline aggregates are subjected to pure tension using mixed homogeneous boundary conditions. Tension is prescribed along direction y . The displacement component u_2 is zero at the bottom surface $y=0$ and prescribed at all nodes of the top surface $y=L$, L being the length of the sample. All lateral surfaces, including the constrained surface, are free of forces. As a result of these boundary conditions, for all realizations of the microstructure, all components of the mean stress tensor Σ vanish, except Σ_{22} . The boundary conditions are summarized in figure 7. The grains of the polycrystalline aggregates are taken to be copper single crystals. Their mechanical behaviour is assumed here to be purely elastic. The cubic elasticity of copper single crystals is characterized by the three moduli

$$C_{11} = 168\,400 \text{ MPa}, \quad C_{12} = 121\,400 \text{ MPa}, \quad C_{44} = 75\,390 \text{ MPa} \quad (8)$$

according to [35]. The corresponding value of the anisotropy coefficient $a = 2C_{44}/(C_{11} - C_{12})$ is 3.2. This rather strong anisotropy is responsible for the non-homogeneous deformation of polycrystalline copper aggregates in the elastic regime.

4.2. Influence of mesh size

The finite element mesh size must be sufficiently small to ensure the convergence of the results and large enough to make the computations tractable. Convergence must be tested at both global and local levels. For this purpose, the effect of mesh refinement was studied for one particular 3D polycrystalline aggregate containing 52 grains. Ten different mesh densities were tested for this specific aggregate.

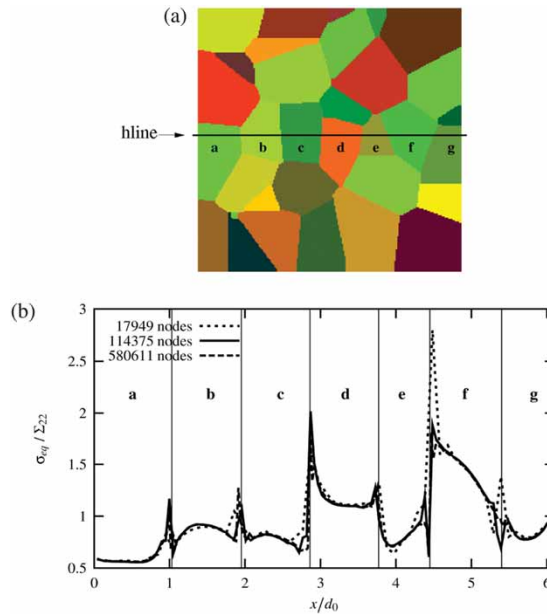


Figure 8. Influence of mesh size on the local stress values: (a) constrained free surface used for the determination of the optimal mesh size; (b) von Mises stress profiles along the line *hline* shown in (a) as a function of the number of nodes of the mesh. In these calculations the morphology and crystal orientations are unchanged but different meshes are used. The vertical lines indicate the x -position of the intersection between grain boundaries and line *hline*. Labels have been attributed to the grains crossed by *hline*.

The number of degrees of freedom is equal to the number of nodes multiplied by three, i.e. the number of displacement components. It was varied from 53 847 for the coarsest mesh up to 1741 833 for the finest one. For each computation an apparent Young's modulus can be defined as

$$E^{\text{app}} = \frac{\Sigma_{22}}{E_{22}} = \frac{\langle \sigma_{22} \rangle}{\langle \varepsilon_{22} \rangle} \quad (9)$$

The apparent Young's modulus was studied as a function of mesh size in [31]. The analysis shows the convergence of the apparent Young's modulus for increasing number of degrees of freedom. For more than 100 000 degrees of freedom, the apparent Young's modulus does not vary by more than 0.3%.

Since we are interested in an accurate description of the intragranular mechanical fields, the convergence of the results with respect to mesh density must also be tested at the local level. For that purpose, the normalized stress profiles along a line on a free surface were plotted for the same aggregate and three mesh refinements in figure 8. The differences mainly arise close to grain boundaries. To ensure a proper description of these critical regions, a mesh density of 11 300 d.o.f. per grain on average was finally chosen, which is an intermediate value between the two finest meshes used in this section. As a result, the number of degrees of freedom in the

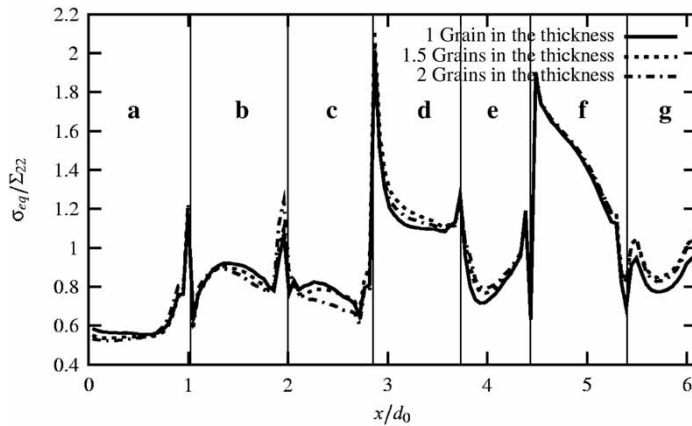


Figure 9. Effect of the average number of grains in the thickness on the local von Mises equivalent stress level normalized by the global mean stress plotted along the line *hline* of figure 8a. The position along the x -axis is x and d_0 is the mean grain size of the considered microstructure. The vertical lines indicate the x -position of the intersection between grain boundaries and line *hline*.

computations presented in the sequel is proportional to the number of grains considered.

4.3. Number of grains within the thickness

The sample thickness is also the result of a compromise. The number of grains within the thickness must be large enough for the stress–strain field at the constrained free surface to be practically unaffected by a further increase of the thickness. It must however be kept as small as possible for the computation to remain tractable. This section therefore addresses a longstanding question of the mechanics of polycrystals: What is the range of stress–strain fields in polycrystals? This question is treated here in the case of anisotropic elasticity. The question can be rephrased as follows. For a polycrystalline lamella in tension with a given free surface of observation, it is intuitive that the stress–strain field at this surface will become stationary as the sample thickness is gradually increased. What is the critical thickness and the corresponding number of grains required to reach this stationary field? For that purpose, three polycrystalline aggregates sharing the same surface $z=0$ but with distinct thicknesses were taken out of the same 3D microstructure image:

- one grain in the thickness on average (in fact 0.7 grain on average), leading to a mesh containing $60 \times 60 \times 7$ quadratic elements, i.e. 343 125 d.o.f.
- 1.5 grains in the thickness on average (in fact 1.4 grains on average), leading to a mesh containing $60 \times 60 \times 14$ quadratic elements, i.e. 653 127 d.o.f.
- two grains in the thickness on average (in fact 2.1 grains on average), leading to a mesh containing $60 \times 60 \times 21$ quadratic elements, i.e. 963 129 d.o.f.

The three samples were subjected to simple tension and the resulting stress fields at the free surface were observed. Figure 9 shows the corresponding equivalent von Mises stress profiles along a line belonging to the constrained free surface. The local stress values turn out to only slightly depend on the sample thickness. The differences obtained for 1.5 and 2 grains within the thickness are less than 3%. In the computations presented in this work, the sample thickness will therefore be kept to two grains within the thickness on average. This result indicates that the spatial range of elastic stresses is rather low. Its order of magnitude is of about two grains.

Finally, the 17 realizations of polycrystalline microstructures with the constrained surface geometry of figure 1 are meshed according to the mesh density determined in section 4.2. This corresponds to a mesh containing $60 \times 60 \times 21$ quadratic elements, i.e. 963 129 d.o.f. These meshed microstructures are two grains thick on average and contain 85 grains on average with a variance of nine grains.

5. Ensemble averaging stress fields at a given surface of elastic copper polycrystals

The results of the 17 tensile tests performed numerically on the polycrystalline aggregates with a constrained free surface are presented and commented. The ensemble average and variance operators are then applied to the stress field at the constrained free surface. This gathered information fully characterizes the sensitivity of surface grains to their 3D environment.

5.1. Stress–strain heterogeneities at the common free surface

The applied mean strain E_{22} was 0.01. However, within the framework of linear elasticity, normalized stress distributions contain the whole information that can be extracted from the computations. The normalized von Mises equivalent stress maps at the constrained free surface are shown for four random polycrystalline aggregates in figures 10a–d.

The first striking feature of all the simulations is that stress concentrations systematically occur close to grain boundaries which represent the main sources of strain incompatibilities in anisotropic elastic polycrystals. Stress concentration factors greater than 2.3 are observed at the free surface near grain boundaries. As a result, the stress distribution patterns are intimately related to the grain morphology. This feature of polycrystalline anisotropic elasticity has been documented in the literature especially in the case of cubic and hexagonal symmetry: cubic elasticity in [36, 37], zinc polycrystals in [29, 38] and zirconium alloy polycrystals in [24]. This effect is not an artifact due to the multiphase element meshing technique, as checked, e.g. in [22, 24, 37, 39]. Note also that the zones with enhanced stress levels generally extend far beyond the first row of elements close to the grain boundaries and affected by the multiphase element technique.

The second striking result of these simulations is the strong differences observed in the stress fields at the constrained free surface from one realization to another. In the realization of figure 10d, the local stress concentration factors in grain 27 are mostly lower than 1.5. In contrast, a large zone of stress concentration larger than 2 is observed in the same grain in realization 10c. Almost one half of grain 23 displays stress concentration factors higher than 1.5 in the realizations 10a–c.

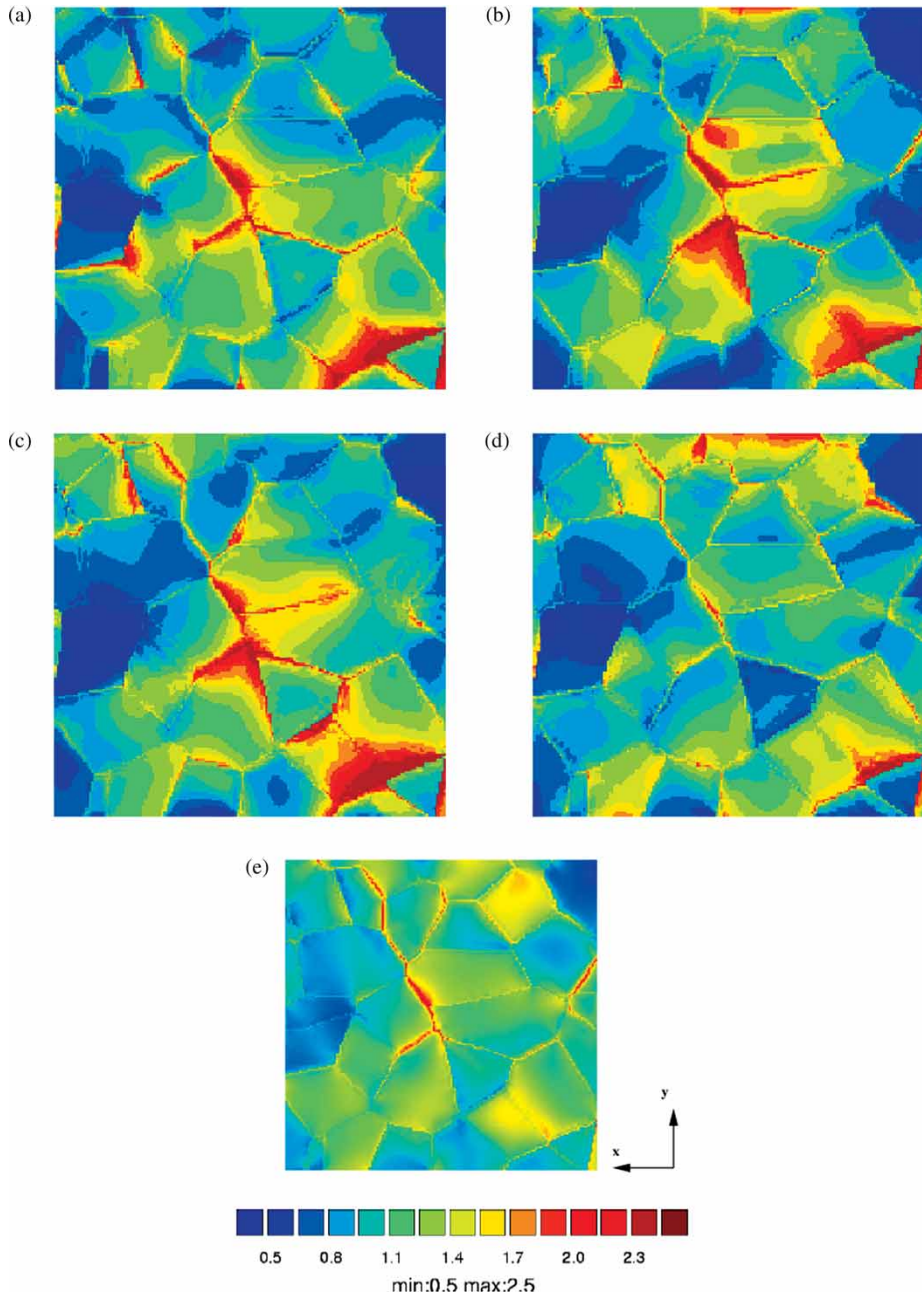


Figure 10. Von Mises equivalent stress maps at the reference free surface for four different polycrystalline aggregates subjected to pure tension (a)–(d). The stress distribution is normalized by the global ensemble average stress $\overline{\Sigma_{22}}$ over all realizations. The reference free surface is that of figure 1. Panel (e) shows the result obtained for the aggregate made of columnar grains (figure 5). Tension is applied along the y -direction.

They are always smaller than 1.4 in the same grain for the realization 10d. The stress fields have common features, in particular a strong strain incompatibility at the junction between the grains 22–27–28–23–18 situated in the middle of the surface. It must be recalled that the initial crystal orientation of all the surface grains 1–39 of figure 1 is the same in all the finite element computations. As a result, the differences in stress observed at the free surface from one realization to another are solely due to the variation of grain shape below the surface.

Figure 10e shows the stress concentration map obtained with the columnar grains of figure 5. The stress field is found to be smoother than for the random polycrystals. In particular, it is more homogeneous inside the grains. Stress concentration takes place at several grain boundaries but the extent of strain incompatibility is significantly smaller than for the random polycrystals. Minimal and maximal values are found to be closer to each other in this columnar polycrystal. Note that

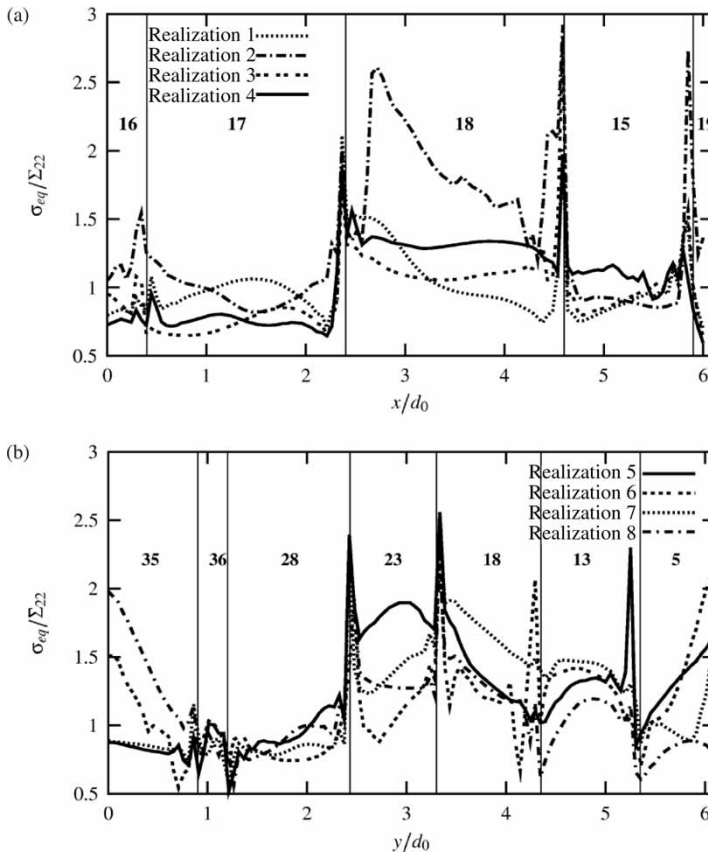


Figure 11. Equivalent von Mises stress profiles along the lines *hline* (a) and *vline* (b) of figure 1 for eight different realizations of polycrystalline aggregates with a constrained free surface and subjected to pure tension. The stress distribution is normalized by the global ensemble average stress $\bar{\Sigma}_{22}$ over all realizations. The reference free surface is given in figure 1. The vertical lines indicate the x -position of the intersection between grain boundaries and line *hline*. The labels of the grains crossed by *hline* and *vline* are indicated.

the same finite element meshes have been used for the columnar and random microstructures so that no bias is introduced by the mesh.

The fluctuations from one realization to another can be analyzed more quantitatively by plotting the stress concentration values along the horizontal line *hline* and the vertical line *vline* of figure 1. These profiles are shown in figures 11a and b for eight realizations. The positions of the grain boundaries crossed by the two lines are marked by vertical lines in the plots. The stress peaks close to grain boundaries are clearly visible. The stress level is almost constant along *hline* in the large grains 17 and 18 for realizations 1, 3 and 4. In contrast, a steep stress gradient is observed in the same grains for realization 2. The reason for such differences is the difference in grain geometry. This fact will be illustrated in detail by comparing the different environments of a specific grain in section 4 of part 2 of this work in the case of linear and nonlinear behaviour [27]. Pronounced stress gradients are generally characteristic of smaller grain segments, especially along *vline*. In a given grain, the average stress level can vary by a factor of 2 from one realization to another. A systematic statistical analysis of these results is presented in the next subsection.

5.2. Ensemble averages and dispersion

Each material point $P(\mathbf{x})$ of the constrained free surface of figure 1 experiences various stress states depending on the specific realization. In statistical physics, one usually considers the ensemble average of the phase state at a material point and the corresponding variance [40–42]. In this work, we present the ensemble averaged field of von Mises equivalent stresses $\overline{\sigma_{eq}}(\mathbf{x})$ computed according to formula (4) where $N=17$ has to be substituted. A schematic view of this ensemble averaging procedure is shown in figure 12.

The map of the ensemble averaged field of von Mises equivalent stresses at the free surface is shown in figure 13a. As a result of the averaging process, the ensemble averaged stress field is smoother than for the individual realizations. However, stress concentrations still remain with values ranging from 0.3 to 4. The averaged

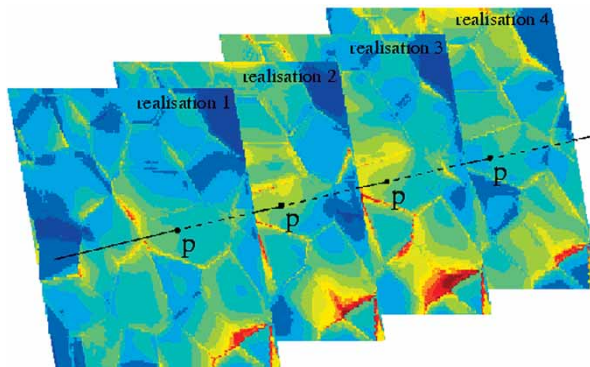


Figure 12. Schematic view of the ensemble averaging procedure. The ensemble averaged stress field is obtained by averaging the local stress value reached at the same geometrical point P belonging to the constrained free surface for all considered realizations.

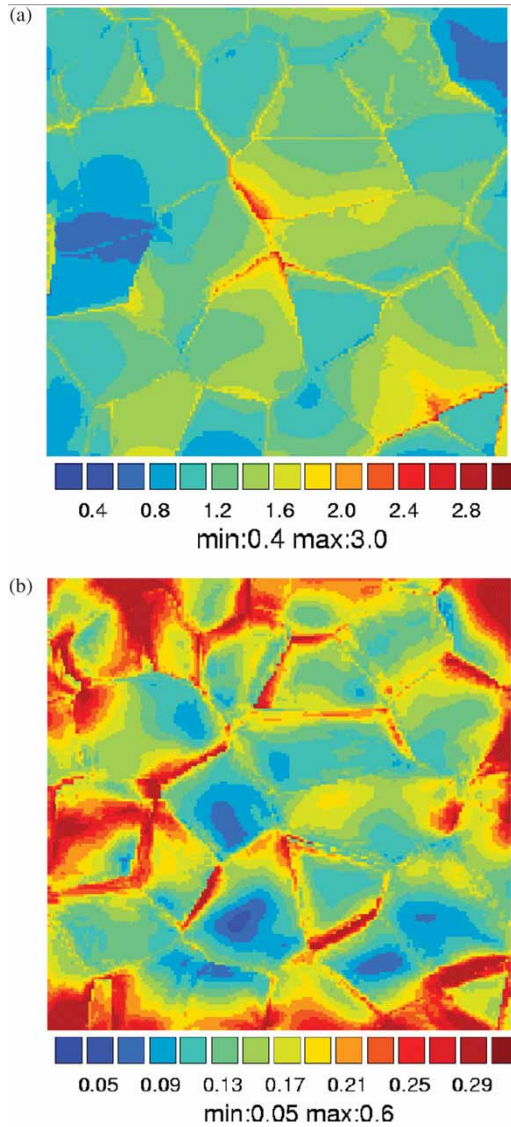


Figure 13. (a) Ensemble average of the von Mises equivalent stress field $\overline{\sigma_{\text{eq}}(\mathbf{x})}/\overline{\Sigma_{22}}$ at the imposed free surface of the polycrystalline aggregates in tension. (b) Field of the relative variance $D(\sigma_{\text{eq}}(\mathbf{x})/\overline{\sigma_{\text{eq}}(\mathbf{x})})$ of the local von Mises equivalent stress at the imposed free surface. Tension is applied in the direction y . The y -direction is vertical in this figure.

stress field is not quasi-uniform, because the grain morphology and the crystal orientations at the free surface do not vary from one realization to another. The obtained averaged stress field therefore reveals the main effect of grain boundaries of the free surface. This corresponds to a kind of effective behaviour of the observed surface. For comparison, the same averaging procedure has been applied

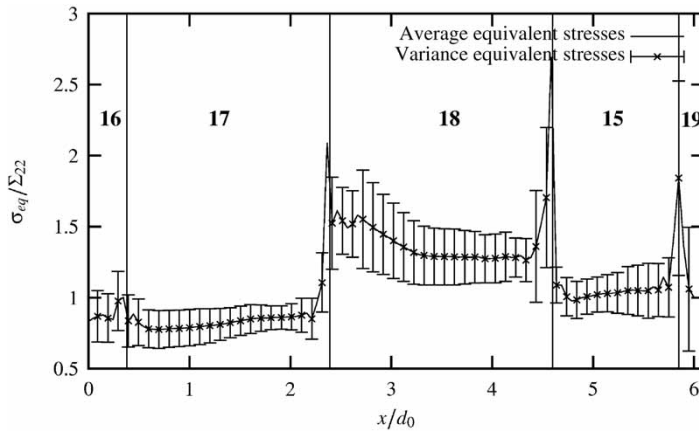


Figure 14. Ensemble average and relative variance of the von Mises equivalent stress field along the line *hline* of figure 1. The stress values are normalized by the ensemble average $\overline{\Sigma_{22}}$ of the mean axial stress for all samples.

to the rear free surface $z = H$ where both grain shape and grain orientation vary from one realization to another. In this case, the averaged stress field is uniform and equal to $\overline{\Sigma_{22}}$ with fluctuations smaller than 5% which correspond to a relative variance of $\epsilon = 0.05/\sqrt{17} = 1.2\%$ in the estimation of the mean. The found mean apparent stiffness is in fact an estimation of the effective behaviour of copper polycrystals [37]. The ensemble averaged stress map of figure 13(a) shows a central zone of the free surface, made of the grains 27–28–23–18, where the stress concentration factors are the highest, reaching values as high as 2 to 2.5. It can be noted also that the mixed homogeneous conditions applied at the top and bottom do not introduce artificially high stress concentrations on average. The same holds for the lateral free surfaces.

Figure 14 shows the ensemble averaged equivalent stress along line *hline*. The stress turns out to be rather homogeneous in the five grains crossed by the line. The stress concentration factors take the values 0.8, 1.3 and 1. Grain 18 is the most deformed one on average. The high stress levels in some grains indicate that stress concentration does not occur close to grain boundaries only.

The ensemble averaged stress field is to indicate in which grains of the given surface the probability of strong stress concentration is the highest. In the context of experimental strain field measurements, this map gives the most relevant zone for the deposition of a microgrid [2, 43].

The most interesting result of these computations is the map of the relative variance of local stresses $D(\overline{\sigma_{eq}}(\mathbf{x}))/\overline{\sigma_{eq}}(\mathbf{x})$, shown in figure 13(b). This map shows that, locally, the stress level can fluctuate around the mean value from 5% up to 60%, from one realization to another. These are the minimal and maximal values of the local relative variance. Two main sources of dispersion can be recognized. Firstly, the grain boundaries, as already noticed, are sources of stress variations from one realization to another. Most regions close to grain boundaries are red in the map of figure 13b. This can be explained by the fact that the change in position of grain boundary plane below the surface from one realization to another leads to the

strongest variations of local stress levels. Secondly, the top and bottom lines where the displacement boundary conditions are prescribed also display high levels of stress variance. The constrained displacement associated with the changes of the underlying microstructure leads to marked strain incompatibilities and strongly different local stress levels from one realization to another.

The intervals of confidence plotted on the curve giving the ensemble averaged stresses along *hline* in figure 14 show however that large scatter is observed at, but is not limited to grain boundaries. In the core of grains 18 and 15, the local stress concentration factor can vary by $\pm 20\%$ from one realization to another. The relative variance also gives information about the precision of the estimated ensemble average field. By dividing the local relative variance of the stress by $\sqrt{17}$, the square-root of the number of considered realizations, according to standard theory of samples, an estimation of the precision in the evaluation of the local mean is obtained. In the blue regions of the figure 13b, the precision in the evaluation of the local stress level given in figure 13a is better than 2.5%. In contrast, in the red regions where large fluctuations were observed, the precision may not be better than 7%. If an improved precision is wanted, a larger number of realizations must be considered.

The stress field obtained for columnar grains shown in figure 10e is rather similar to the smooth ensemble average field of figure 13a for random microstructures. However, this cannot be seen as a general result since similar computations with different lattice orientations should be performed. In particular, this statement does not hold in the case of elastoplasticity. This will be shown in part 2 [27].

6. Conclusions

The main conclusions of the first part of this work are the following:

- Polycrystalline aggregates containing 85 grains on average with different grain shapes and crystal orientations, except at one free surface where the 2D grain shape and initial lattice orientation were fixed *a priori*, have been constructed based on 3D image analysis. The obtained morphology does not significantly depart from standard Voronoi tessellation. The algorithm can be applied to real images of equiaxial grains obtained by EBSD.
- Seventeen samples having one free surface with 39 grains in common have been subjected to overall tensile deformation assuming an anisotropic elastic response of the grains and taking the cubic elastic moduli of pure single crystal copper into account. The equivalent von Mises stress fields at the free surface with fixed microstructure were ensemble averaged in order to determine the regions where the presence of high stresses is most probable. High stress levels are observed in a central region of the surface close to five grain boundaries. In anisotropic elasticity, strain incompatibilities between grains systematically result in higher equivalent stresses close to grain boundaries, whatever the shape of the 3D grains.
- The variance of the surface stress field from one realization to another gives a field information about fluctuations. A confidence interval of $\pm 20\%$ around

the local average can be attached to most material points at the free surface, even far from grain boundaries. Higher fluctuations of more than 40% and reaching 60% are generally observed close to grain boundaries.

- A columnar grain morphology was considered in the analysis as a reference frequently used in the literature in the absence of information on 3D grain morphology. In the special case of the constrained 2D microstructure, the equivalent stress field induced by the tensile deformation of the columnar grains was found to be smoother than for random 3D grain shapes. This stress field is quite similar to the ensemble averaged stress field obtained from the 17 random aggregates, especially in the central zone with high stress levels.

The morphology of underlying grains in the volume has a major impact on the local stress–strain fields obtained on a given polycrystalline free surface in anisotropic elasticity. This is a question often raised in the interpretation of strain field measurements at the surface of deformed polycrystals. Considering only one special realization introduces a bias in the detection of the region of high stress levels. Considering only a columnar microstructure leads to an underestimation of stress gradients. Even though most authors are aware of the role that 3D grain morphology may play in the development of stress fields at a free surface, no quantitative assessment of these fluctuations was available in the literature.

The stress field from a linear analysis can be used to predict the inception of plastic slip in metal polycrystals. The links between elastic strain incompatibilities from grain to grain and the onset of plasticity have been studied from the experimental point of view for instance in [44]. The analysis of elastic strain fields can also be used to assess the quality of recent homogenization based polycrystal models providing estimations of mean fields but also of fluctuations in elastic polycrystalline aggregates [45]. One may expect from this elasticity analysis that the activation of slip systems during subsequent plastic deformation of the material will differ significantly from one realization to another. It is the objective of the second part of this work to quantitatively assess the fluctuations in the plastic strain field observed at a given free surface by changing the 3D grain morphology of the underlying microstructure [27].

References

- [1] R. Becker, *Acta Metall. Mater.* **39** 1211 (1991).
- [2] L. Allais, M. Bornert, T. Bretheau, *et al.*, *Acta Mater.* **42** 3865 (1994).
- [3] A. Ziegenbein, H. Neuhäuser, J. Thesing, *et al.*, *J. Phys. IV France* **8** Pr8-407 (1998).
- [4] G. Mohamed, B. Bacroix, T. Ungar, *et al.*, *Mat. Sci. Engng.* **A234–236** 940 (1997).
- [5] F. Delaire, J.L. Raphanel, and C. Rey, *Acta Mater.* **48** 1075 (2000).
- [6] F. Eberl, S. Forest, T. Wroblewski, *et al.*, *Metall. Mater. Trans.* **33A** 2825 (2002).
- [7] R. Parisot, S. Forest, A.-F. Gourgues, *et al.*, *Comput. Mater. Sci.* **19** 189 (2001).
- [8] N. Mary, V. Vignal, R. Oltra, *et al.*, *Phil. Mag.* **85** 1227 (2005).
- [9] J. Mandel, *Plasticité Classique et Viscoplasticité*, volume 97 of CISM Courses and Lectures (Springer-Verlag, Berlin, 1971).
- [10] R.J. Asaro, *J. Appl. Mech.* **50** 921 (1983).

- [11] C. Teodosiu, J. Raphanel, and L. Tabourot, in *Large Plastic Deformations MECAMAT'91*, edited by C. Teodosiu and F. Sidoroff (Balkema, Rotterdam, 1993), pp. 153–158.
- [12] P. Eriean and C. Rey, *Int. J. Plast.* **20** 1763 (2004).
- [13] K.S. Cheong and E.P. Busso, *Acta Mater.* **52** 5665 (2005).
- [14] H. Miyamoto, in *First International Conference on Structural Mechanics in Reactor Technology* (Springer-Verlag, Berlin, 1972), pp. 535–566.
- [15] R.J. Asaro, *Adv. Appl. Mech.* **23** 1 (1983).
- [16] S.V. Harren and R.J. Asaro, *J. Mech. Phys. Solids* **37** 191 (1989).
- [17] F. Havlicek, J. Kratochvil, M. Tokuda, *et al.*, *Int. J. Plast.* **6** 281 (1990).
- [18] R. Becker and S. Panchanadeeswaran, *Acta Metall. Mater.* **43** 2701 (1995).
- [19] A.J. Beaudoin, P.R. Dawson, K.K. Mathur, *et al.*, *Int. J. Plast.* **11** 501 (1995).
- [20] G.B. Sarma, B. Radhakrishnan, and T. Zacharia, *Comput. Mater. Sci.* **12** 105 (1998).
- [21] F. Barbe, L. Decker, D. Jeulin, *et al.*, *Int. J. Plast.* **17** 513 (2001).
- [22] F. Barbe, S. Forest, and G. Cailletaud, *Int. J. Plast.* **17** 537 (2001).
- [23] A. Bhattacharyya, E. El-Danaf, S.R. Kalidindi, *et al.*, *Acta Metall. Mater.* **17** 861 (2001).
- [24] O. Diard, S. Leclercq, G. Rousselier, *et al.*, *Int. J. Plast.* **21** 691 (2005).
- [25] J. Crépin, T. Bretheau, D. Caldemaison, *et al.*, *Acta Mater.* **48** 505 (2000).
- [26] A. Musienko, Large deformation and damage in crystal plasticity. PhD thesis, Ecole des Mines de Paris, 2005.
- [27] A. Zeghadi, S. Forest, A.-F. Gourgues, *et al.*, Ensemble averaging stress–strain fields in polycrystalline aggregates with a constrained free surface microstructure – Part 2: Crystal plasticity. *Phil. Mag* this issue (2007).
- [28] A.J. Schwartz, M. Kumar, and B.L. Adams, *Electron Backscatter Diffraction in Materials Science* (Kluwer Academic, Plenum Publisher, New York, 2000).
- [29] R. Parisot, S. Forest, A. Pineau, *et al.*, *Metall. Mater. Trans.* **35A** 797 (2004).
- [30] C. Lantuéjoul, *Geostatistical Simulation: Models and Algorithms* (Springer, Berlin, 2002).
- [31] A. Zeghadi, Effets de la morphologie tri-dimensionnelle et de taille de grain sur comportement mécanique d'agrégats polycristallins. PhD thesis, Ecole des Mines de Paris, 2005.
- [32] N. Lippmann, T. Steinkopff, S. Schmauder, and P. Gumbsch, *Comput. Mater. Sci.* **9** 28 (1997).
- [33] F. Feyel, S. Calloch, D. Marquis, *et al.*, *Comput. Mater. Sci.* **9** 141 (1997).
- [34] Z-set package, www.nwnumerics.com, www.mat.ensmp.fr. (2001).
- [35] B. Gairola and E. Kröner, *Int. J. Engng Sci.* **19** 865 (1981).
- [36] S. Quilici and G. Cailletaud, *Comput. Mater. Sci.* **16** 383 (1999).
- [37] M. Nygård, *Mech. Mater.* **35** 1049 (2003).
- [38] F. Barbe, R. Parisot, S. Forest, *et al.*, *J. de Physique IV* **11** Pr5-277 (2001).
- [39] O. Diard, S. Leclercq, G. Rousselier, *et al.*, *Comput. Mater. Sci.* **25** 73 (2002).
- [40] M.J. Beran, *Statistical Continuum Theories* (Interscience Publishers, New York, 1968).
- [41] E. Kröner, *Statistical Continuum Mechanics*, CISM Course, (Springer Verlag, Vienna, 1972).
- [42] D. Jeulin and M. Ostojca-Starzewski, *Mechanics of Random and Multiscale Microstructures*, volume 430, CISM Lecture Notes (Springer Verlag, Berlin, 2001).
- [43] P. Doumalin, M. Bornert, and J. Crépin, *Mécanique et Industries* **4** 607 (2003).
- [44] K. Hashimoto and H. Margolin, *Acta Metall.* **31** 773 (1983).
- [45] N. Letouzé, R. Brenner, O. Castelnau, *et al.*, *Scripta Mater.* **47** 595 (2002).